



**HAL**  
open science

## A microfluidic strategy for accessing the thermal conductivity of liquids at different temperatures

Rosa Moreno Jimenez, Benoit Creton, Claire Marliere, Lionel Teule-gay,  
Olivier Nguyen, Samuel Marre

► **To cite this version:**

Rosa Moreno Jimenez, Benoit Creton, Claire Marliere, Lionel Teule-gay, Olivier Nguyen, et al.. A microfluidic strategy for accessing the thermal conductivity of liquids at different temperatures. *Microchemical Journal*, 2023, 193, pp.109030. 10.1016/j.microc.2023.109030 . hal-04155254

**HAL Id: hal-04155254**

**<https://hal.science/hal-04155254>**

Submitted on 7 Jul 2023

**HAL** is a multi-disciplinary open access archive for the deposit and dissemination of scientific research documents, whether they are published or not. The documents may come from teaching and research institutions in France or abroad, or from public or private research centers.

L'archive ouverte pluridisciplinaire **HAL**, est destinée au dépôt et à la diffusion de documents scientifiques de niveau recherche, publiés ou non, émanant des établissements d'enseignement et de recherche français ou étrangers, des laboratoires publics ou privés.



16 **Abstract:**

17 Biomass-based biofuels represent a promising alternative fossil energy source, for which conversion  
18 processes - mostly performed at high pressure and temperature conditions - require thermophysical  
19 property data, particularly thermal conductivity. Conventional methods to measure thermal  
20 conductivity are often time consuming and/or need important quantities of products. Microfluidics  
21 has been proven to be a viable solution to these issues thanks to its low reagent consumption, fast  
22 screening capabilities, improvement of heat and mass transfers etc. However, microfabrication  
23 materials used in previous works, do not exhibit sufficient chemical inertness, nor thermomechanical  
24 properties to apply such methods to large ranges of fluids systems and conditions. Here, we develop  
25 new microreactors including sensors integrated into microfluidic channels with an operating principle  
26 based on the transient thermal offset approach for thermal conductivity measurement, built with  
27 materials commonly used for microreactors operated in harsh conditions. The sensor calibration is  
28 performed on water/ethanol mixtures and externally validated for two fluids: n-pentadecane and  
29 ethan-1,2-diol along with the evolution of their thermal conductivity with temperature. Finally, the  
30 microfluidic device is used to generate thermal conductivity data for 2,5-dimethylfuran, a biomass-  
31 based compound with high potential as biofuel and for which experimental data has not been  
32 reported so far.

33 **Keywords:** Micro-sensor; Microfluidics; Thermal conductivity; Temperature

## 34 **1. Introduction**

35 The thermal conductivity ( $\lambda$ ) of liquids is an essential thermodynamic data for the technical design of  
36 many processes. For instance, transport properties involving mass and heat transfers are widely  
37 considered in industrial applications such as separators, reactors, or even heat exchangers. The  
38 conversion of biomass into useful forms of energy (e.g., biofuels) represents a promising alternative  
39 to fossil resources. In the case of aircraft, the fuel itself serves as the primary heat transfer medium  
40 in the thermal management systems. Thus, fluid's thermal conductivity is an important  
41 thermodynamic data to consider when designing and developing processes that will produce  
42 alternative fuels.

43 There are various experimental techniques available for the measurement of thermal conductivity,  
44 the transient hot-wire method is regarded as one of the standard macroscopic techniques for fluid  
45 samples [1,2]. This technique is based on monitoring temperature changes of a thin metallic wire.  
46 The wire and then the surrounding liquid begin to heat up when applying a constant electric power.  
47 The thermal conductivity of the surrounding liquid can be determined by recording the temporal and  
48 spatial evolution of the corresponding temperature response. Two components can be used to  
49 monitor temperature changes: a heater, which is made of a resistive metal wire or film, and  
50 thermocouples, which are used for temperature sensing [3,4]. Nevertheless, due to the low thermal  
51 conductivities of liquids in comparison with solids or metals, the thermocouple must be placed very  
52 close to the heating element, or the duration of the measurements must be sufficiently long, both of  
53 which are challenging to implement. Another solution to monitor temperature changes is by  
54 considering the variation of the electrical resistance of the wire or film in contact with the fluid. The  
55 wire or film can be used in this case, both as heating element and temperature sensor as already  
56 proposed Gustafsson et al. [5–7]. Instead of a wire, other geometries such as thin metal sheets; as  
57 the transient hot strip (THS) method [5] or double spirals with insulating materials have also been  
58 implemented such as transient plane source (TPS) method [8]. The TPS method uses a geometry with  
59 higher surface contact than the hot strip or hot wire method, which are also more fragile, and

60 temperature measurements can be performed with greater sensitivity and accuracy. Besides  
61 transient methods used to determine the thermal parameters there are approaches based on  
62 harmonic (sinusoidal) excitation called the  $3\omega$  method [9]. However, this technique requires  
63 supplementary instruments which can be costly, as well as complex installations for the  
64 measurement.

65 However, due to convection and radiation that accompany heat losses, it is challenging to precisely  
66 determine thermal conductivity using these methods with large equipment; therefore, using smaller  
67 scales volumes would limit these issues. Thus, milli or microfluidics have been shown to be  
68 interesting approaches for such measurements [10–12]. Besides being smaller, lighter, and cheaper  
69 than conventional instruments, microfluidics can greatly reduce the measurement times along with  
70 reduced reagent consumption, resulting in a significant financial and industrial impact specially when  
71 fluid sample is costly or scarcely available.

72 Several microfluidics based methods were proposed including separated heating element such as a  
73 laser which uses localized heating source along to reduce undesired heat loss [13] and temperature  
74 sensor such as miniature thermocouples [13–15]. The resistive element in microtechnology, is a thin  
75 film structure deposited on a substrate with known thermal properties. As a result, the use of MEMS  
76 (MicroElectroMechanical Systems) has enabled the adaptation of traditional methods to determine  
77 thermal conductivity at micro-scales. Therefore, it was already reported that the thermal  
78 conductivity can be measured using a single resistive element that acted as both heater  
79 and temperature sensor, such as the hot-strip method [16,17] or the  $3\omega$  method [18,19], for which  
80 the sensor implemented is simpler to fabricate.

81 Oudebrouckx et al. reported the use of micro-scale devices to predict the thermal conductivity of  
82 fluids [20]. The authors used aluminium as a highly thermally conductive material that acted as heat  
83 sink to eliminate uncertainties encountered in micro-scale systems. The bottom of the device was  
84 made of polyimide, an electrically insulating substrate, with a metal resistive heating structure. The  
85 term "thermal penetration depth" refers to the distance that the heat flux travels through the

86 material from any point on the thin metallic film's surface [3,21]. When working with small liquid  
87 samples, thermal depth issues frequently cause additional measurement errors. They deliberately  
88 applied thermal pulses that exceeded the liquid's physical boundaries inside the microchannel, while  
89 staying within the limits of the aluminum top reference. As the top reference material has a much  
90 higher thermal effusivity than the substrate and fluid, the heat dissipated by the sensor structure is  
91 absorbed, ensuring a constant temperature increase rates for all subsequent measurements. The  
92 thermal conductivity of fluids from transient curves can be calculated using simple data analysis.  
93 However, only a few fluids have been experimentally measured in the cited works, and some of the  
94 considered microfabrication materials exhibit limited chemical compatibility and are only suitable for  
95 room temperature measurements. The temperature dependence of fluid thermal conductivity has  
96 only been documented in a few studies that only measured one fluid (DI water) [22,23].

97 The silicon-borosilicate microfluidic technology [24] has become popular over the past decade as it  
98 allows extending the range of operating conditions compared to conventional microfluidics  
99 materials. This characteristic has opened the microfluidic fields of research to materials synthesis  
100 [25], chemistry in harsh conditions [26], geosciences [27,28] and particularly for determining the  
101 thermo-physical properties of fluid systems under pressure and temperature [10,27]. This technology  
102 is beneficial for real-world applications, especially in industrial settings. Therefore, we propose the  
103 development of a new microfluidic device that allows to determine thermal conductivity for various  
104 chemical families and different temperature conditions up to 60°C.

105 In this paper, we demonstrate the use of silicon-borosilicate microreactors equipped with thin film  
106 sensors to measure the thermal conductivity of several fluids in the range 20-60°C. We first detail  
107 briefly the fluids and materials used, the conception of the microfluidics device, the overall  
108 measurement setup, the readout device used to measure fluid's thermal conductivity, and the  
109 measurement procedure. Then, the obtained results are discussed, including the microdevice  
110 calibration on microliter-sized samples of water/ethanol mixtures, the validation measurements  
111 performed on well-known fluids (n-pentadecane and ethan-1,2-diol), and the acquisition of new

112 experimental data for 2,5-dimethylfuran, which is one typical product issued from the conversion of  
113 biomass. Further developments and perspectives are finally discussed.

## 114 **2. Materials and methods**

### 115 **2.1. Chemicals and materials.**

116 Mixtures of ethanol/ water were made using absolute ethanol (99.8%) and distilled water. The fluids  
117 selected for thermal conductivity measurements: ethanol, ethan-1,2-diol, n-pentadecane, with high  
118 purity grades, were purchased from Alfa Aesar, and 2,5-dimethylfuran from Sigma Aldrich.

119 Silicon wafers (1 mm thick, diameter: 4 inches) covered with a silicon oxide (SiO<sub>2</sub>) layer of 500 nm  
120 thickness, as well as Pyrex® (borosilicate glass, 1.5 mm thick, diameter: 2 inches) were used for the  
121 conception of the microfluidic chip.

122 Buffered oxide etchant (BOE) and a tetramethylammonium hydroxide solution (25 wt. % in H<sub>2</sub>O)  
123 were purchased from Sigma Aldrich. MICROCHEM remover PG N-Methyl-2-pyrrolidone (NMP) based  
124 solvent was provided by Fisher Scientific.

125 Commercial targets from Neyco (diameter: 2 inches and thickness: 3mm) of Chrome and Platinum  
126 with purities of 99,997 % were used for the Magnetron-sputtering deposition of the sensors on the  
127 Pyrex wafer.

### 128 **2.2. Microfluidic device fabrication.**

129 The microfluidic device including sensors integrated into microchannel was fabricated following a  
130 three-step procedure. First, microchannels were etched on a silicon substrate using photolithography  
131 and wet etching techniques, as previously described [24]; then, the sensors were created on a  
132 borosilicate glass substrate surface by selectively depositing a structured metallic film patterned  
133 according to the microchannels features; finally, the silicon and borosilicate glass substrates were  
134 assembled using a fusion bonding process resulting in the final microfluidic device. These procedures  
135 are detailed in the Supporting Information ESI-1 section.

136 ***Choice of microchannel and sensor geometry.*** The microchannels and sensors were designed using  
137 the AutoCAD® software and printed on flexible photomasks. As shown in Figure 1, the main

138 microchannel is 200  $\mu\text{m}$  wide and 60  $\mu\text{m}$  deep, the measurement micro-pool has dimensions of 2  
 139 mm x 3 mm. This design enables the micro-pool to encompass the sensor, allowing the fluid to  
 140 completely cover it. Spiral shape was chosen due to its high surface contact, uniform thermal  
 141 distribution, and high resistance, resulting in lower power consumption [29]. The spiral shaped metal  
 142 structure has a 2 mm diameter with 6 concentric rings, each having a width and spacing of 50  $\mu\text{m}$  and  
 143 100  $\mu\text{m}$ , respectively. The fabricated microfluidic device is illustrated in Figure 1.

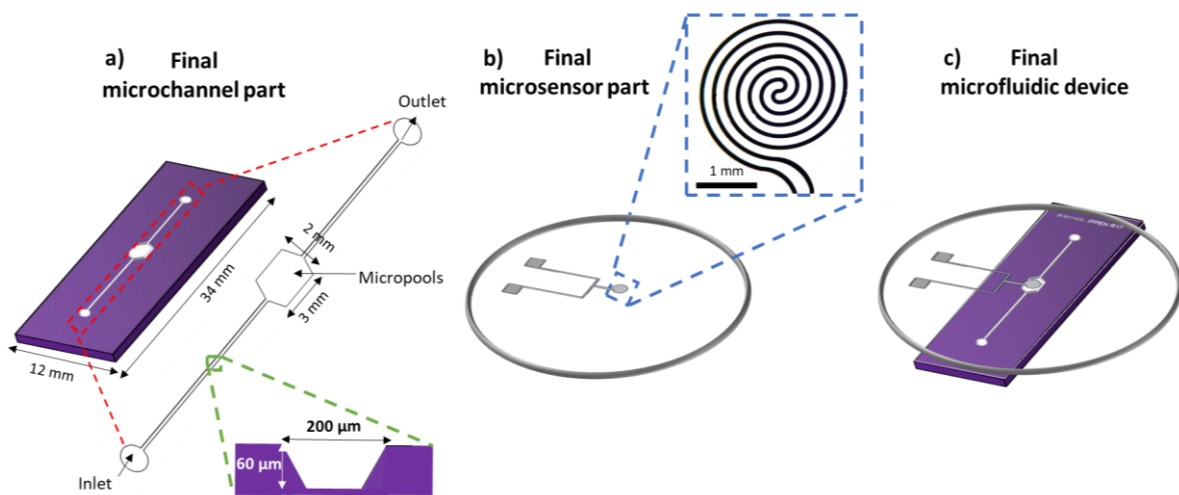


Figure 1: Illustration of the dimensions and geometries for a) the microchannel part: red dotted rectangle represents a zoom of the microchannel (micro-pool), green dotted rectangle represents the cross-section microchannel's trapezoidal geometry and b) sensor part: blue dotted square represents a zoom of the spiral shape metallic structure, c) illustration of the final microfluidic device

144 The scheme of its cross-section is proposed in Figure 2. The bottom part of the device consists in a  
 145 thermal/electrical insulator (borosilicate glass substrate) on which a Pt thin film spiral planar heating  
 146 structure is present. The top of the microchannel is made of a thermal conductor top reference  
 147 (silicon substrate). Due to its high thermal conductivity, silicon was specifically chosen. This device is  
 148 conceptually advantageous due to its chemical inertia, the ability to work at higher temperatures and  
 149 optical access for coupling to other *in situ* characterization.

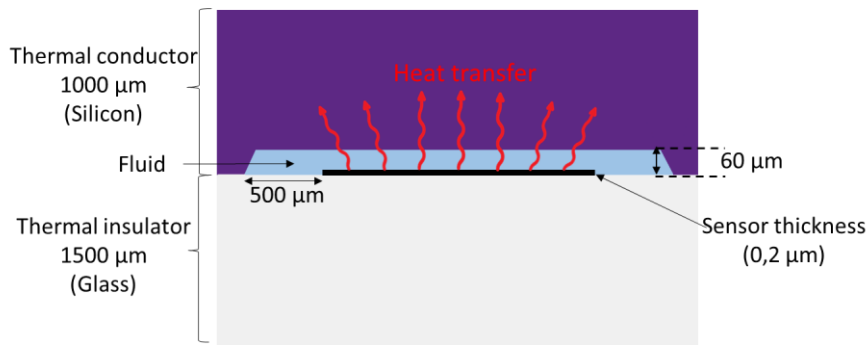


Figure 2: A schematic cross-section of the microfluidic cavity designed for measurements of fluids  $\lambda$ . Heat transfer generated by metallic spiral is represented by red arrows.

150 The as-obtained microfluidic device must be then connected to the experimental environment  
 151 through a compression piece “holder” [30]. The electric interfaces are connected via square contact  
 152 pads on both ends of the heater, and the temperature is monitored using a K-type thermocouple  
 153 (probe diameter = 0.3 mm) placed in-between the holder and the microfluidic device, as detailed in  
 154 the Supporting Information ESI-2 section.

### 155 2.3. Thermal conductivity measurement

156 A Wheatstone bridge was used in the  $\lambda$  measurement system [31–34] to monitor the electrical  
 157 resistance variation of the thin Pt spiral sensor. When the bridge is balanced, small voltage variations  
 158 can be translated into temperature variations, as discussed further below.

159 **Description of the set-up.** The schematic measurement system (available in Supporting Information  
 160 Figure ESI-3-1) consists in a DC power with constant voltage supplied by a generator from RS Pro  
 161 model RS6005P. The Wheatstone bridge consists in two precision resistors:  $R_1 = R_2 = 465.8 \Omega$ , with  
 162 an accuracy of 0.01% at room temperature. The thin film sensor's electrical resistance ( $R_S$ ) has an  
 163 initial value at the selected temperature labelled as  $R_{init}$ .  $R_v$  is a variable resistor set using a  
 164 precision resistance decade box from Guildline Instruments model 9346/10k $\Omega$  with a resolution of  
 165 0.01  $\Omega$ , used to balance the bridge ( $R_v = R_{init}$ ). A Voltcraft-655 BT multimeter with a sampling  
 166 frequency of 64 Hz and a measuring range of 10 mV was used to acquire the unbalanced DC voltage  
 167  $\Delta V$  (between  $V_a$  and  $V_b$ ).

168 **Measurement protocol.** A syringe pump (Fisherbrand™ KDS100) is used to inject the fluid sample  
 169 inside the microreactor. The liquids are fed to the microdevice at a flowrate of 10 μL/s with steps of  
 170 200 μL injection per measurement. Apart from these flushes, the fluid in the micro-pool remains  
 171 static inside the microdevice. Once the fluid is loaded inside the microchamber, the relay is switched  
 172 to the bridge. The Wheatstone bridge is initially balanced under a negligible current (<1.0 mA) to  
 173 avoid any sensor's heating, the voltage measured has to be maintained around zero, which  
 174 corresponds to the  $R_{init}$  of the sensor.  
 175 The thin metallic spiral is used as a Joule heating element. However, depending on the sensor's  $R_{init}$ ,  
 176 the voltage and current sent must be slightly tuned to ensure that all applied pulses have the same  
 177 power regardless of the sensors, allowing comparison of each sensor's response. Equation (1), is used  
 178 to determine the amount of current ( $I$ , in A) needed to produce a desired power ( $P$ , in W).

$$I = \sqrt{\frac{P}{R_{init}}} \quad (1)$$

179 Then, the desired DC power is applied to the sensor. As the temperature increases, the electrical  
 180 voltage between the bridge's ends changes, and small resistance increments can be measured. The  
 181 voltage at the bridge end's is measured , and the resistance of the sensor ( $R_s$ ) is deduced from  
 182 equation (2) [35].

$$\Delta V = \left( \frac{R_s}{R_2 + R_s} - \frac{R_v}{R_1 + R_v} \right) \times V_0 \quad (2)$$

183 Where  $V_0$  is the DC supply voltage.

184 The temperature of the microsensor is calculated from the resistance measurements using the  
 185 experimental values of the variation of the platinum resistivity as a function of temperature. For this  
 186 material, the temperature coefficient of resistance ( $\alpha$ ) was determined experimentally ( $\alpha =$   
 187  $3.01 \times 10^{-3} \pm 0.21 \times 10^{-3} K^{-1}$ ). The use of this coefficient allows to convert the measured  
 188 electrical resistance into a temperature variation ( $T - T_{ref}$ ) using equation (3) [36].

$$R_s = R_{ref}[1 + \alpha(T - T_{ref})] \quad (3)$$

189 Where  $T$  is the temperature of the sensor,  $R_{ref}$  is the electrical resistance at temperature  $T_{ref}$ . The  
190 temperature change of the sensor structure can be plotted as a function of  $\sqrt{t}$ , using equation (4) as  
191 already reported by Gustavsson *et al.* and Harris *et al.* [7,37], and a linear fit can be made once the  
192 value of  $\Delta T$  reaches the equilibrium.

$$\Delta T(t) = s\sqrt{t} \quad (4)$$

193 When sensor is sufficiently heated its temperature response should approach linearity when plotted  
194 versus the square root of time (available in Supporting Information Figure ESI-3-2). The first non-  
195 linear portion at the beginning of the squared root trend curve, which is attributed to the substrate  
196 effect, is ignored in data processing [7]. In the linear part, the slope ( $s$ ) is related to the Silicon top  
197 reference acting as a heat sink. The silicon top material should be thicker than the microchannel  
198 depth, so that it acts as a semi-infinite medium during a heating step [5]. This implies that the linear  
199 portion of the curves – sensor temperature responses – are anticipated to be parallel regardless of  
200 the thermal properties of the fluid inside the micro-pool. The measured slopes constant values at the  
201 end of each sensor response indicate that the thermal penetration depth is adequate [23], so all  
202 uncertainties are eliminated.

### 203 **3. Results and discussion**

204 We report hereafter the experimental results obtained using the micro-sensor implemented within  
205 the microfluidic device. This section is composed of three parts: first, the calibration of the sensor  
206 response to fit the thermal behaviour of well-known fluids mixtures; second, an external validation of  
207 the sensor calibration for two fluids; and finally, new experimental values for a biomass by-product  
208 for which there is a lack of thermal conductivity data information in the literature.

#### 209 **3.1. Sensor calibration: water/ethanol mixtures.**

210 Several microfluidic devices were produced using the fabrication procedure described in the previous  
211 section. For each device, the initial electrical resistance of the sensor at room temperature was

212 measured, and  $R_{init}$  values ranging from 480  $\Omega$  to 620  $\Omega$  were determined, roughly corresponding to  
213 the resistance of the thin Pt spirals, which are about  $200 \pm 20$  nm thick. The calibration of the  
214 microfluidic devices shown below is the result of three separate sensor calibrations, each with three  
215 repeatability measurements. The calibration of each sensor was performed using different  
216 water/ethanol mixtures for which thermal conductivity  $\lambda$  values are experimentally known. Indeed,  
217 the use of these two liquids in mixture that are harmless and easily accessible allows a wide range of  
218 liquid  $\lambda$  values to be covered, from 0.180 to 0.603 W/(m.K). The considered volume fractions of  
219 ethanol in mixtures were as follows: 0% (pure water), 25%, 50%, 75%, and 100% (pure ethanol).  
220 Reference  $\lambda$  values were obtained from the literature [38][39], and are reported in Supporting  
221 Information Table ESI-4-1. Digital signal processing of the sensor response allows time changes in  
222 resistance to be expressed as temperature changes, and curve's offsets converted in  $\lambda$  values.  
223 Several parameters inherent to the device may be set to improve the accuracy of  $\lambda$  values obtained  
224 during experimental measurements. Among them we investigated: (i) the electrical power applied  
225 during heating, (ii) the duration of the heating pulse, and (iii) the selection of the time interval for the  
226  $\lambda$  calculation.

227 We investigated heating power values from 30mW to 90mW. To ensure that all sensors deliver the  
228 same heating power during the pulse, the electrical current is adapted by considering equation (1)  
229 together with the determined sensor  $R_{init}$  value. In practice, we can assume that the sensor's  
230 accuracy increases with heating power. However, applying too much heating power may result in  
231 disadvantages such as local vaporization of the liquid and bubble formation, or even sensor failure.  
232 Indeed, the risk of the sensor deteriorating and being damaged increases above 60 mW. Figure 3  
233 shows the temperature response curves obtained for the considered water/ethanol mixtures,  
234 applying a heating power of 60 mW. Curves for other investigated heating powers are available in  
235 Supporting Information Figures of section ESI-4. Note that a heating power of 30mW was found not  
236 sufficient to distinguish between some of the water/ethanol mixtures and did not lead to proper  
237 similar slopes for all of them. At 40 mW, it resulted in different offsets for mixtures, but different

238 slopes were still observed. At 50 mW, slopes became similar and useable for the  $\lambda$  calculation. For  
 239 our proposed microfluidic sensor device, we determined that a heating power of 60 mW ( $60.03 \pm$   
 240  $0.42$  mW) is appropriate and was therefore considered for the measurements, unless specified  
 241 otherwise.

242 The duration of the heat pulses must be chosen to ensure that the thermal energy reaches the limits  
 243 of the static fluid sample within the microcavity. In practice, it could be considered that accuracy  
 244 improves with pulse duration. However, after a certain period, the temperature of the fluid does not  
 245 rise as much because the silicon top reference, dissipates the heat acting as heat sink. We  
 246 investigated heating pulse durations from 15 s to 60 s. Figure 3 shows the temperature response  
 247 curves for the water/ethanol mixtures applying a heating pulse of 60 s. Clearly, a heat pulse greater  
 248 than 12 s (corresponding to  $3.5 \text{ s}^{1/2}$  on Figure 3) appears mandatory, which means that for shorter  
 249 measurement times, the heat flow has not covered the distance between the heater and the silicon  
 250 substrate ( $59.8 \mu\text{m}$ ). To have a sufficient integration period for data treatment with the proposed  
 251 microfluidic device, we considered a heat pulse duration of 60 s was appropriate and this value will  
 252 be used hereafter, unless specified otherwise.

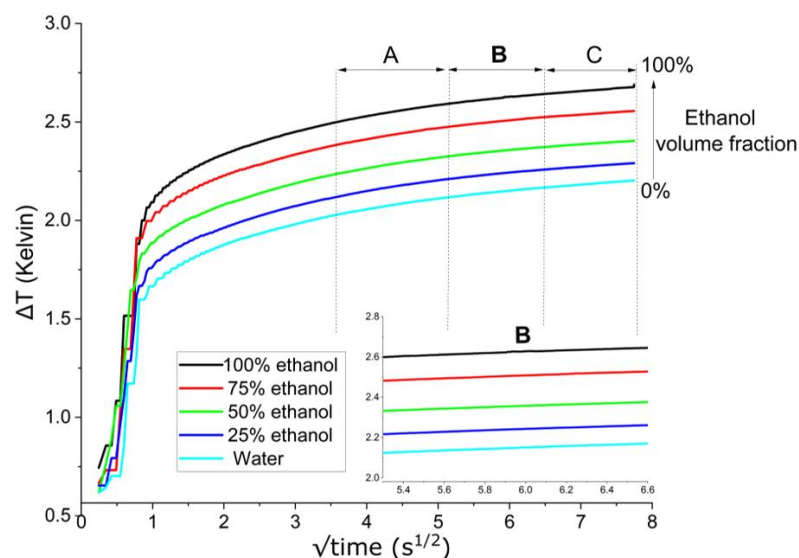


Figure 3: Time variations of the temperature in the microcavity filled with water/ethanol mixtures, when a heat pulse (60 mW during 60 s) is applied to the heater/sensor. A, B, and C stand for three different intervals each having a 16 s duration.

253 The time interval of the curve used to derive temperature variations which are then related to  $\lambda$   
254 values must be carefully fixed. In practice, it can be assumed that the greater the time interval (close  
255 to the end of the curve), the greater the accuracy. However, the local slope of the curve decreases  
256 with time along with the  $\Delta T$  values. Linear regressions were performed on the obtained temperature  
257 response curves for the water/ethanol mixtures (Figure 3), over subsets of the time interval [ $3.5 \text{ s}^{1/2}$   
258 ;  $7.7 \text{ s}^{1/2}$ ]: the time interval was divided into three, each having a duration of 16 s, *i.e.*, A: [ $3.5 \text{ s}^{1/2}$  ;  
259  $5.3 \text{ s}^{1/2}$ ], B: [ $5.3 \text{ s}^{1/2}$  ;  $6.6 \text{ s}^{1/2}$ ], and C: [ $6.6 \text{ s}^{1/2}$  ;  $7.7 \text{ s}^{1/2}$ ]. While the slopes obtained for interval A  
260 are similar across mixtures, these values are about twice as high as those derived for intervals B and  
261 C, indicating that heat flux has not yet reached the liquid boundary. In these two latter cases, we  
262 found appropriate to use B as the time interval, temperature variations are expected to be greater  
263 with B than with C, leading to a better accuracy.

264 From the curves shown in Figure 3 the offset value from linear regressions performed in the interval  
265 B [ $5.3 \text{ s}^{1/2}$  ;  $6.6 \text{ s}^{1/2}$ ] were extracted and related to the thermal conductivity  $\lambda$  of the corresponding  
266 water/ethanol mixtures. Depending on the sensor, the slopes obtained from linear fits at [ $5.3 \text{ s}^{1/2}$  ;  
267  $6.6 \text{ s}^{1/2}$ ] ranges from 0.028 to 0.035.

268 Depending on the composition of the water/ethanol mixture, the  $\Delta T$  value caused by a heat pulse  
269 ranges from 1.9 K to 2.5 K. In the investigated time interval, the variation of the offset values with  
270 thermal conductivities can be assumed as a linear model ( $R^2 = 0.992$ ) with offset =  $a \cdot \lambda + b$ . The a and  
271 b values obtained for each sensor are reported in Supporting Information Table ESI-5-1. The so-  
272 obtained expression stands for the calibration curve available in Supporting Information Figure ESI-5-  
273 1. Note that Oudebrouckx *et al.* suggested the use of an exponential relation between the  
274 temperature offset and  $\lambda$ . However, such fitting curves are not adapted to our microfluidic device  
275 and operating conditions. Moreover, the use of a linear relation between the offset and  $\lambda$  makes the

276 uncertainty on the determination of  $\lambda$  constant over the whole range. Finally, it should be noticed  
277 that due to the variability of the parameters a and b among sensors, it is not possible to establish a  
278 universal curve applicable to all sensors.

### 279 **3.2. Sensor calibration: external validation.**

280 Two fluids with known experimental thermal conductivity behaviours were selected to perform the  
281 validation of the microfluidic device, i.e. fluids not used to set the calibration curve. First an  
282 hydrocarbon, n-pentadecane having at 293.15 K a  $\lambda$  value of 0.137 W/(m.K), slightly outside of the  
283 calibration curve. The results obtained for this fluid should lead to conclusions about extrapolations  
284 from the calibration curve. Then, an oxygenated fluid, ethan-1,2-diol having at 293.15 K a  $\lambda$  value of  
285 0.255 W/(m.K), which is within the calibration curve's range, but with a more pronounced non-linear  
286 trend in  $\lambda$  with temperature variations than other fluids.

287 For each fluid, measurements were performed using the three sensors and then, the  $\lambda$  values were  
288 determined by applying the corresponding calibration curve. Values of  $\lambda$  measured for n-  
289 pentadecane and ethan-1,2-diol at 293.15 K are detailed in the Supporting Information Table ESI-5-2.  
290 For n-pentadecane, the values obtained for  $\lambda$  range between 0.128 and 0.138 with a mean value of  
291 0.134 W/(m.K). This latter is in good agreement with the reference experimental value of 0.137  
292 W/(m.K) [40]. This external validation point demonstrates that calibration curves can be extrapolated  
293 to  $\lambda$  values lower – or higher offset values – than the range covered by water/ethanol mixtures. For  
294 ethan-1,2-diol, the  $\lambda$  measured values range between 0.290 and 0.316 with a mean value of 0.303  
295 W/(m.K). The observed systematic deviation of about 20% from the reference experimental value of  
296 0.255 W/(m.K) [41] is unsatisfactory and appear to be similar to data from the DIPPR database [42]  
297 that was not considered for correlations settings. Searching for artefacts inherent to our  
298 experiments, we investigated property correlations [43] and properties differences between ethan-  
299 1,2-diol and other fluids considered in this work. It highlighted dissimilarities primarily in viscosity, for  
300 instance the value for ethan-1,2-diol (21 mPa.s) is about one order of magnitude higher than the  
301 value for water (1.0 mPa.s), ethanol (1.2 mPa.s), and n-pentadecane (2.5 mPa.s), at 293.15 K [42,43].

302 This would suggest that heat transfer by convection is not so negligible in microfluidics, and in our  
 303 case,  $\lambda$  measurements are accurate for the range of viscosity values covered by fluids used during  
 304 calibration.

305 The variation of  $\lambda$  with the temperature was then investigated for n-pentadecane and ethan-1,2-diol.  
 306 The obtained values are presented in Table 1 and Figure 4 compares the obtained values to those  
 307 suggested by the literature [40–43]. For n-pentadecane, the good agreement observed with respect  
 308 to reference  $\lambda$  values at 293.15 K are confirmed at 313.15 and 333.15 K, with a mean absolute  
 309 relative deviation of about 8%. This validates the ability of our microfluidics device as well as our  
 310 approach to be used to quantitatively predict the  $\lambda$  of liquids. Regarding ethan-1,2-diol, similarly to  
 311 observations done at 293.15 K, our measured  $\lambda$  values overestimate reference values at 313.15 and  
 312 333.15 K. It can be noticed that the trend observed with temperature variations – ranging from  
 313 293.15 and 333.15 K – agrees with that of the reference values.

314 Table 1: *Thermal conductivity (W/(m.K)) values measured for the n-pentadecane and ethan-1,2-diol using our*  
 315 *microfluidic device, for temperature ranging from 293.15 to 333.15 K.*

	n-pentadecane	ethan-1,2-diol
293.15 K	0.134 ± 0.019	0.303 ± 0.028
313.15 K	0.125 ± 0.024	0.303 ± 0.027
333.15 K	0.111 ± 0.026	0.305 ± 0.027

316

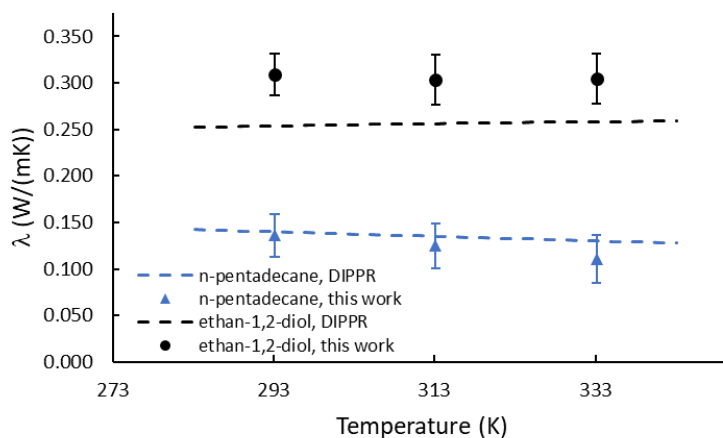


Figure 4: The evolution of  $\lambda$  value as a function of temperature for n-pentadecane (blue) and ethan-1,2-diol (black). Experimental values obtained in this work for n-pentadecane (triangles) and ethan-1,2-diol (circles) are compared to predictions using DIPPR's correlations (dashed lines).

### 3.3. Thermal conductivity data for 2,5-dimethylfuran.

The biomass can be seen as a raw material from which high-value products can be derived. For instance, cellulose present in lignocellulosic biomass can be converted into glucose or fructose, from which compounds with potential as biofuels can be derived, *e.g.* 2,5-dimethylfuran. To our knowledge, there is no experimental  $\lambda$  data for 2,5-dimethylfuran. Therefore, we used our microfluidic device to generate new data points, and each data point is the average result of 10 acquisitions.  $\lambda$  values measured for 2,5-dimethylfuran at 293.15, 313.15 and 333.15 K are reported in Table 2. Indeed, its viscosity value of 0.4 mPa.s at 293.15 K [49,50] is similar to that of fluids used to during sensors calibrations.

Figure 5 shows a comparison between our data points and the predicted evolutions of the  $\lambda$  value as a function of temperature for 2,5-dimethylfuran using two models: one available from the DIPPR [42] and one proposed by Chung *et al.* [44]. It can be noticed that the two predictive models overestimate our experimental data, and that the trends observed with temperature – ranging from 293.15 to 333.15 K – reasonably agree. Based on our experimental data and temperature ranges, we can suggest the use of a linear model to estimate the thermal conductivity 2,5-dimethylfuran as a function of temperature, as follow:

$$\lambda = -4.25 \times 10^{-4} T + 0.24542,$$

with T the temperature.

Table 2: Thermal conductivity (W/(m.K)) values measured for 2,5-dimethylfuran at 293.15, 313.15 and 333.15 K.

$\langle \lambda \rangle$	293.15 K	313.15 K	333.15 K
$\lambda$	$0.120 \pm 0.018$	$0.114 \pm 0.015$	$0.103 \pm 0.021$

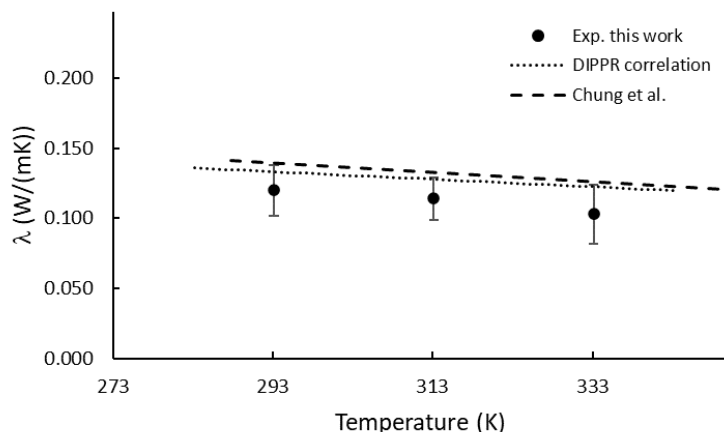


Figure 5: The evolution of  $\lambda$  value as a function of temperature for 2,5-dimethylfuran. Experimental values from this work are compared to predictions using DIPPR's correlations (dashed line) and the model by Chung et al. [44] (dotted line).

#### 337 4. Conclusion

338 We investigated the use of materials commonly employed for microfluidic reactors compatible with  
 339 harsh processes conditions to develop a new microdevice for  $\lambda$  measurements, with an operating  
 340 principle based on the transient thermal offset approach. The microfluidics device, including a sensor  
 341 integrated into a microchannel, was fabricated following a three-step procedure: microfluidic  
 342 channels were etched on a silicon substrate using photolithography / wet etching techniques;  
 343 sensors were created on a borosilicate glass substrate surface by depositing a spiral shaped metal  
 344 thin film; the silicon and borosilicate glass substrates were assembled using a fusion bonding process.  
 345 The sensor response was calibrated by fitting the thermal behaviours of well-known water/ethanol  
 346 mixtures. We decided to set the heating power, the length of the heating pulse, and the time interval  
 347 for  $\lambda$  calculations to 60mW, 60 s and [28 s ; 44 s], respectively. The microfluidic device and its settings  
 348 were then externally validated on two fluids: n-pentadecane and ethan-1,2-diol, for temperatures  
 349 ranging from 293.15 to 333.15 K. Finally, we generated new experimental  $\lambda$  values for 2,5-  
 350 dimethylfuran.

351 We demonstrated that existing thermal conductivity measurement devices can be miniaturized, by  
 352 considering microfluidic procedures and using silicon as heat sink on one side/surface of the micro-

353 chip. The manufactured microdevice enables to carry out experiments under high pressure and  
354 temperature conditions. Besides the use of inert materials such as silicon and borosilicate open ways  
355 to measure thermal conductivity values for various chemical families and to allow direct observation  
356 of fluids, which is of interest for coupling measurements with other in situ characterizations  
357 techniques. We investigated the temperature effect on thermal conductivity for fluids containing  
358 hydrocarbons and oxygenated compounds. Future works will examine pressure effects on the  $\lambda$  of  
359 liquids given that the silicon/borosilicate technology can be used in a wide range of pressure and  
360 temperature conditions. Considering that these effects are generally negligible for pressures below  
361 about 50 bar [45], the microdevice – and more specifically the measurement micro-cavity – will have  
362 to be redesigned to withstand pressures well above this limit. Since the proposed design places the  
363 sensor in direct contact with the fluid, the future deposition of thin protective films made of inert  
364 glasses on top of the sensors could open ways to expand this approach to more aggressive chemicals.

365

#### 366 **Acknowledgements**

367 Authors gratefully thank Drs Pascal Mougín, Leonel Lira Cortés and Saul Garcia Duarte for the helpful  
368 scientific discussions and Philippe Pauvert and Hervé Failla for the instrumentation support.

369 **References**

- 370 [1] J.J. Healy, J.J. de Groot, J. Kestin, The theory of the transient hot-wire method for measuring  
371 thermal conductivity, *Physica B+C* 82 (1976) 392–408. [https://doi.org/10.1016/0378-](https://doi.org/10.1016/0378-4363(76)90203-5)  
372 4363(76)90203-5.
- 373 [2] Y. Nagasaka, A. Nagashima, Simultaneous measurement of the thermal conductivity and the  
374 thermal diffusivity of liquids by the transient hot-wire method, *Review of Scientific Instruments*  
375 52 (1981) 229–232. <https://doi.org/10.1063/1.1136577>.
- 376 [3] A. Franco, An apparatus for the routine measurement of thermal conductivity of materials for  
377 building application based on a transient hot-wire method, *Applied Thermal Engineering* 27  
378 (2007) 2495–2504. <https://doi.org/10.1016/j.applthermaleng.2007.02.008>.
- 379 [4] C. Gobbé, S. Iserna, B. Ladevie, Hot strip method: application to thermal characterisation of  
380 orthotropic media, *International Journal of Thermal Sciences* 43 (2004) 951–958.  
381 <https://doi.org/10.1016/j.ijthermalsci.2004.02.002>.
- 382 [5] S.E. Gustafsson, E. Karawacki, M.N. Khan, Transient hot-strip method for simultaneously  
383 measuring thermal conductivity and thermal diffusivity of solids and fluids, *J. Phys. D: Appl.*  
384 *Phys.* 12 (1979) 1411–1421. <https://doi.org/10.1088/0022-3727/12/9/003>.
- 385 [6] S.E. Gustafsson, Transient plane source techniques for thermal conductivity and thermal  
386 diffusivity measurements of solid materials, *Review of Scientific Instruments* 62 (1991) 797–804.  
387 <https://doi.org/10.1063/1.1142087>.
- 388 [7] M. Gustavsson, E. Karawacki, S.E. Gustafsson, Thermal conductivity, thermal diffusivity, and  
389 specific heat of thin samples from transient measurements with hot disk sensors, *Review of*  
390 *Scientific Instruments* 65 (1994) 3856–3859. <https://doi.org/10.1063/1.1145178>.
- 391 [8] A. Maqsood, N. Amin, M. Maqsood, G. Shabbir, A. Mahmood, S.E. Gustafsson, Simultaneous  
392 measurements of thermal conductivity and thermal diffusivity of insulators, fluids and  
393 conductors using the transient plane source (TPS) technique, *Int. J. Energy Res.* 18 (1994) 777–  
394 782. <https://doi.org/10.1002/er.4440180903>.

- 395 [9] D.G. Cahill, Thermal conductivity measurement from 30 to 750 K: the  $3\omega$  method, Review of  
396 Scientific Instruments 61 (1990) 802–808. <https://doi.org/10.1063/1.1141498>.
- 397 [10] T. Gavaille, N. Pannacci, G. Bergeot, C. Marliere, S. Marre, Microfluidic approaches for accessing  
398 thermophysical properties of fluid systems, React. Chem. Eng. 4 (2019) 1721–1739.  
399 <https://doi.org/10.1039/C9RE00130A>.
- 400 [11] A.M. Streets, Y. Huang, Chip in a lab: Microfluidics for next generation life science research,  
401 Biomicrofluidics 7 (2013) 11302. <https://doi.org/10.1063/1.4789751>.
- 402 [12] D. Sinton, Energy: the microfluidic frontier, Lab Chip 14 (2014) 3127–3134.  
403 <https://doi.org/10.1039/c4lc00267a>.
- 404 [13] S.R. Choi, D. Kim, Measurement of thermal properties of microfluidic samples using laser point  
405 heating thermometry, Thermochimica Acta 455 (2007) 11–15.  
406 <https://doi.org/10.1016/j.tca.2006.11.035>.
- 407 [14] C. Offenzeller, M. Knoll, T. Voglhuber-Brunnmaier, M.A. Hintermuller, B. Jakoby, W. Hilber, Fully  
408 Screen Printed Thermocouple and Microheater Applied for Time-of-Flight Sensing in  
409 Microchannels, IEEE Sensors J. 18 (2018) 8685–8692.  
410 <https://doi.org/10.1109/JSEN.2018.2868161>.
- 411 [15] D. Kuvshinov, M.R. Bown, J.M. MacInnes, R.W.K. Allen, R. Ge, L. Aldous, C. Hardacre, N. Doy,  
412 M.I. Newton, G. McHale, Thermal conductivity measurement of liquids in a microfluidic device,  
413 Microfluid Nanofluid 10 (2011) 123–132. <https://doi.org/10.1007/s10404-010-0652-x>.
- 414 [16] G. Velve Casquillas, M. Le Berre, C. Peroz, Y. Chen, J.J. Greffet, Microlitre hot strip devices for  
415 thermal characterization of nanofluids, Microelectronic Engineering 84 (2007) 1194–1197.  
416 <https://doi.org/10.1016/j.mee.2007.01.187>.
- 417 [17] M. Gustavsson, H. Nagai, T. Okutani, Thermal effusivity measurements of insulating liquids using  
418 microsized hot strip probes, Review of Scientific Instruments 74 (2003) 4542–4548.  
419 <https://doi.org/10.1063/1.1606537>.
- 420 [18] S.R. Choi, J. Kim, D. Kim, 3omega method to measure thermal properties of electrically

- 421 conducting small-volume liquid, *Review of Scientific Instruments* 78 (2007) 84902.  
422 <https://doi.org/10.1063/1.2777162>.
- 423 [19] S.R. Choi, D. Kim, Real-time thermal characterization of 12 nl fluid samples in a microchannel,  
424 *Review of Scientific Instruments* 79 (2008) 64901. <https://doi.org/10.1063/1.2937180>.
- 425 [20] G. Oudebrouckx, T. Vandenryt, S. Bormans, P.H. Wagner, R. Thoelen, Measuring Thermal  
426 Conductivity in a Microfluidic Device With the Transient Thermal Offset (TTO) Method, *IEEE*  
427 *Sensors J.* 21 (2021) 7298–7307. <https://doi.org/10.1109/JSEN.2020.3047475>.
- 428 [21] L. Qiu, Y. Ouyang, Y. Feng, X. Zhang, X. Wang, In vivo skin thermophysical property testing  
429 technology using flexible thermosensor-based  $3\omega$  method, *Int. J. Heat Mass Transf.* 163 (2020)  
430 120550. <https://doi.org/10.1016/j.ijheatmasstransfer.2020.120550>.
- 431 [22] S. Roy-Panzer, T. Kodama, S. Lingamneni, M.A. Panzer, M. Asheghi, K.E. Goodson, Thermal  
432 characterization and analysis of microliter liquid volumes using the three-omega method, *Rev.*  
433 *Sci. Instrum.* 86 (2015) 24901. <https://doi.org/10.1063/1.4907353>.
- 434 [23] R. Karthik, N. Harish Nagarajan, B. Raja, P. Damodharan, Measurement of thermal conductivity  
435 of fluids using 3- $\omega$  method in a suspended micro wire, *J. Engin. Thermophys.* 21 (2012) 60–68.  
436 <https://doi.org/10.1134/S1810232812010067>.
- 437 [24] S. Marre, A. Adamo, S. Basak, C. Aymonier, K.F. Jensen, Design and Packaging of Microreactors  
438 for High Pressure and High Temperature Applications, *Ind. Eng. Chem. Res.* 49 (2010) 11310–  
439 11320. <https://doi.org/10.1021/ie101346u>.
- 440 [25] S. Marre, J. Park, J. Rempel, J. Guan, M.G. Bawendi, K.F. Jensen, Supercritical  
441 Continuous-Microflow Synthesis of Narrow Size Distribution Quantum Dots, *Adv. Mater.* 20  
442 (2008) 4830–4834. <https://doi.org/10.1002/adma.200801579>.
- 443 [26] S. Marre, Y. Roig, C. Aymonier, Supercritical microfluidics: Opportunities in flow-through  
444 chemistry and materials science, *The Journal of Supercritical Fluids* 66 (2012) 251–264.  
445 <https://doi.org/10.1016/j.supflu.2011.11.029>.
- 446 [27] B. Pinho, S. Girardon, F. Bazer-Bachi, G. Bergeot, S. Marre, C. Aymonier, Simultaneous

- 447 measurement of fluids density and viscosity using HP/HT capillary devices, *The Journal of*  
448 *Supercritical Fluids* 105 (2015) 186–192. <https://doi.org/10.1016/j.supflu.2015.04.016>.
- 449 [28] S. Morais, A. Cario, N. Liu, D. Bernard, C. Lecoutre, Y. Garrabos, A. Ranchou-Peyruse, S. Dupraz,  
450 M. Azaroual, R.L. Hartman, S. Marre, Studying key processes related to CO<sub>2</sub> underground  
451 storage at the pore scale using high pressure micromodels, *React. Chem. Eng.* 5 (2020) 1156–  
452 1185. <https://doi.org/10.1039/D0RE00023J>.
- 453 [29] Z.E. Jeroish, K.S. Bhuvaneshwari, F. Samsuri, V. Narayanamurthy, Microheater: material, design,  
454 fabrication, temperature control, and applications—a role in COVID-19, *Biomed. Microdevices* 24  
455 (2021) 3. <https://doi.org/10.1007/s10544-021-00595-8>.
- 456 [30] Theo Gavaille, Methodologies pour la caractérisation de propriétés thermodynamiques dans  
457 des systèmes microfluidiques. Thèse de doctorat, Université de Bordeaux, 2019.
- 458 [31] W. Guo, G. Li, Y. Zheng, C. Dong, Measurement of the thermal conductivity of SiO<sub>2</sub> nanofluids  
459 with an optimized transient hot wire method, *Thermochimica Acta* 661 (2018) 84–97.  
460 <https://doi.org/10.1016/j.tca.2018.01.008>.
- 461 [32] G.-Y. Jeong, S.P. Jang, H.-Y. Lee, J.-C. Lee, S. Choi, S.-H. Lee, Magnetic-Thermal-Fluidic Analysis  
462 for Cooling Performance of Magnetic Nanofluids Comparing With Transformer Oil and Air by  
463 Using Fully Coupled Finite Element Method, *IEEE Trans. Magn.* 49 (2013) 1865–1868.  
464 <https://doi.org/10.1109/TMAG.2013.2245411>.
- 465 [33] D.-W. Oh, Thermal Conductivity Measurement of Liquids by Using a Suspended Microheater, *Int*  
466 *J Thermophys* 38 (2017). <https://doi.org/10.1007/s10765-017-2278-7>.
- 467 [34] J. Maroofi, S.H. Hashemabadi, Experimental and numerical investigation of parameters  
468 influencing anisotropic thermal conductivity of magnetorheological fluids, *Heat Mass Transfer*  
469 55 (2019) 2751–2767. <https://doi.org/10.1007/s00231-019-02618-w>.
- 470 [35] K. Hoffmann, Applying the Wheatstone Bridge Circuit, HBM S1569–11 en, HBM, Darmstadt,  
471 Ger., 2001.
- 472 [36] J. Whitfield, *Electrical craft principles 1*, fourth. ed., Stevenage, Herts, 1995.

- 473 [37] A. Harris, S. Kazachenko, R. Bateman, J. Nickerson, M. Emanuel, Measuring the thermal  
474 conductivity of heat transfer fluids via the modified transient plane source (MTPS), *J Therm Anal*  
475 *Calorim* 116 (2014) 1309–1314. <https://doi.org/10.1007/s10973-014-3811-6>.
- 476 [38] D. R. Lide, *CRC handbook of chemistry and physics*, 81st ed. (CRC, New York 2000).
- 477 [39] A.O. Guimarães, F.A.L. Machado, E.C. da Silva, A.M. Mansanares, Thermal Effusivity and Thermal  
478 Conductivity of Biodiesel/Diesel and Alcohol/Water Mixtures, *Int J Thermophys* 33 (2012) 1842–  
479 1847. <https://doi.org/10.1007/s10765-012-1280-3>.
- 480 [40] Bogatov, G.F., Rastorguev, Yu.L., Grigor'ev, B.A., *Khim. Tekhnol. Topl. Masel*, 14, 9, 31 (1969).
- 481 [41] L. Riedel, *Forsch. Geb. Ing. Wes.*, 11, 6, 340 (1940).
- 482 [42] R.L. Rowley, W.V. Wilding, A. Congote, N.F. Giles, The Use of Database Influence Factors to  
483 Maintain Currency in an Evaluated Chemical Database, *Int J Thermophys* 31 (2010) 860–874.  
484 <https://doi.org/10.1007/s10765-010-0706-z>.
- 485 [43] J.C. Bloxham, M.E. Redd, N.F. Giles, T.A. Knotts, W.V. Wilding, Proper Use of the DIPPR 801  
486 Database for Creation of Models, Methods, and Processes, *J. Chem. Eng. Data* 66 (2021) 3–10.  
487 <https://doi.org/10.1021/acs.jced.0c00641>.
- 488 [44] T.H. Chung, M. Ajlan, L.L. Lee, K.E. Starling, Generalized multiparameter correlation for nonpolar  
489 and polar fluid transport properties, *Ind. Eng. Chem. Res.* 27 (1988) 671–679.  
490 <https://doi.org/10.1021/ie00076a024>.
- 491 [45] G. Latini, Thermophysical properties of fluids: dynamic viscosity and thermal conductivity, *J.*  
492 *Phys.: Conf. Ser.* 923 (2017) 12001. <https://doi.org/10.1088/1742-6596/923/1/012001>.
- 493

- 494 - **Rosa Moreno Jimenez** received her M.Sc degree (2020) in Analytical chemistry from University of  
495 Claude Bernard Lyon 1. She was a research engineer-in-training at Total Energies where she  
496 developed chemometrics techniques, enabling the automation and interpretation of analytical  
497 data. She is currently pursuing the Ph.D. degree in Physical chemistry at IFP Energies Nouvelles.  
498 Her current research focuses on the development of a microfluidic device for the thermal  
499 conductivity measurement of oxygenated compounds under pressure and different temperature  
500 conditions, as well as the acquisition of pre and post-processing experimental data using chemo-  
501 informatics techniques through the development of predictive models.
- 502 - **Benoit Creton** received his M.Sc. degree (2002) from the University of Rennes 1, France, and  
503 his Ph.D. degree (2006) in molecular simulation from the University of Science and  
504 Technology of Lille, France. He then joined the “Thermodynamics and Molecular Simulation”  
505 group at IFP Energies nouvelles as an R&I engineer. His current research focuses on the use of  
506 Chemoinformatics tools from multiscale molecular simulation methods to quantitative  
507 structure–property relationships, to predict property values for complex fluids and advanced  
508 materials. He has published over 50 articles in international Journals.
- 509 - **Claire Marlière** graduated from ESPCI ParisTech in 2010 and received her PhD degree in Materials  
510 Science from Paris-Est University in 2013. She joined IFP Energies nouvelles as a R&I engineer.  
511 After 9 years in the field of energies, Claire recently joined the physical-chemistry group at L’Oréal  
512 as head of lab. Her research focuses on flow of complex fluids, physical chemistry of soft matter,  
513 formulation, emulsion and microfluidics. She has published several articles in international  
514 journals.
- 515 - **Lionel Teulé-Gay** received his M.Sc. degree in physics and engineering from the University of  
516 Grenoble 1, France and joined for 8 years the “Laboratoire de Physique des Gaz et Plasmas”,  
517 CNRS, France. Since 2007 he is an R&I CNRS engineer at the Institute of Condensed Matter  
518 Chemistry of Bordeaux, France. His current research focuses on the development of new

519 devices based on plasma technologies for innovating processes or advanced materials. He has  
520 published over 30 articles in international Journals and he is inventor of 3 patents.

521 - **Olivier Nguyen** is an engineer in the Supercritical Fluids group at the Institute of Condensed  
522 Matter Chemistry of Bordeaux since 1998. He is in charge of the design and layout of different  
523 project's experiments and the maintenance of the equipment. His activities concerns the  
524 microfabrication /development (in the clean room) and the implementation of microreactors and  
525 their coupling with the experimental lab environment. He is also in charge of the mechanical  
526 conception of different system's experiments using CAO and FAO softwares.

527 - **Samuel Marre** received his PhD in Chemical Engineering from the University of Bordeaux in 2006,  
528 before joining the Jensen Lab at MIT as a postdoctoral associate. He is currently a CNRS senior  
529 research at the Institute of Condensed matter chemistry of Bordeaux, head of the supercritical  
530 fluid group. He is a pioneer in the use of high-pressure microfluidic systems for multiple  
531 applications including chemical processes using hydrothermal conditions. He received the CNRS  
532 bronze medal award in 2014 and has published > 80 papers and 7 patents.